INTERNATIONAL JOURNAL FOR NUMERICAL METHODS IN FLUIDS
Int. J. Numer. Meth. Fluids 2013; **00**:1–18
Published online in Wiley InterScience (www.interscience.wiley.com). DOI: 10.1002/fld

Connections between the discontinuous Galerkin method and high-order flux reconstruction schemes

D. De Grazia,[1*] G. Mengaldo,[1*] D. Moxey,[1] P. E. Vincent,[1] S. Sherwin[1]

[1] *Imperial College London, Department of Aeronautics, South Kensington Campus London SW7 2AZ, UK*

SUMMARY

With high-order methods becoming more widely adopted throughout the field of computational fluid dynamics, the development of new computationally efficient algorithms has increased tremendously in recent years. The flux reconstruction approach allows various well-known high order schemes to be cast within a single unifying framework. Whilst a connection between flux reconstruction and the discontinuous Galerkin method has been established elsewhere, it still remains to fully investigate the explicit connections between the many popular variants of the discontinuous Galerkin method and the flux reconstruction approach. In this work, we closely examine the connections between three nodal versions of tensor product discontinuous Galerkin spectral element approximations and two types of flux reconstruction schemes for solving systems of conservation laws on quadrilateral meshes. The different types of discontinuous Galerkin approximations arise from the choice of the solution nodes of the Lagrange basis representing the solution and from the quadrature approximation used to integrate the mass matrix and the other terms of the discretisation. By considering both a linear and nonlinear advection equation on a regular grid, we examine the mathematical properties which connect these discretisations. These arguments are further confirmed by the results of an empirical numerical study. Copyright © 2013 John Wiley & Sons, Ltd.

Received . . .

KEY WORDS: Flux reconstruction; spectral/*hp* element methods; discontinuous Galerkin; tensor product grids; collocation.

1. INTRODUCTION

In recent years there has been much interest in high-order discretisations as they offer the potential to obtain more accurate approximations with less computational cost compared to lower order methods. The most widely adopted high-order methods are based on the discontinuous Galerkin method, introduced by Reed and Hill in 1973 [1]. The DG method is used in both industry and academia due to the computational efficiency of the scheme and attractive numerical properties, and has well-known formulations to cope with both hyperbolic and elliptic problems [2, 3]. Classically the DG method starts with an expression of the underlying problem in a weak form, whereby the governing system is multiplied by a test function and integrated over the domain, which is itself partitioned into non-overlapping elements. A high-order discretisation therefore entails selecting both a basis of polynomials which represent the solution locally on each element and a set of quadrature points on which the inner products arising in the weak formulation can be calculated. Some of the most efficient and ubiquitous forms of the DG method are so-called nodal DG schemes, whereby Lagrange interpolants are combined with a set of nodal solution points on a given element [5].

*Correspondence to: d.de-grazia12@imperial.ac.uk, g.mengaldo11@imperial.ac.uk

	$\mathbf{DG_{SEM}}$-GLL Lumped mass matrix		$\mathbf{DG_{SEM}}$ Exact mass matrix		$\mathbf{DG_{Q>P}}$ Exact mass matrix	
Flux type	Linear	Nonlinear	Linear	Nonlinear	Linear	Nonlinear
$\mathbf{FR_{DG}}$	✗	✗	✓	✓	✓	✗
$\mathbf{FR_{g2}}$	✓	✓	✗	✗	✗	✗

Table I. Connections between different types of DG and FR schemes derived in this work for constant Jacobian elements. ✓ indicates that the schemes are equivalent, whereas ✗ indicates differences between the schemes.

More recently however, another set of methods which are based upon the system being expressed in a differential form have offered an alternative route which avoids the need for quadrature rules, making these schemes easier to implement. The first of these was introduced by Kopriva and Kolias [6] and was extended in 2006 to quadrilateral and triangular elements under the name of spectral-difference (SD) schemes by Liu et al. [8]. Most recently, a new scheme called the flux reconstruction (FR) method was presented by Huynh [4] which has undergone significant development in recent years, with applications to the compressible Euler and Navier-Stokes equations [11, 12], extension from a tensor-product formulation to simplex elements [10], allowing for the use of the method in a wide variety of geometries.

One of the most appealing properties of the FR method is the ability to encapsulate other types of numerical discretisations. Recently a new range of energy stable FR schemes have been identified in [9], referred to as Vincent-Castonguay-Jameson-Huynh (VCJH) schemes. Here, a single real-valued parameter c dictates the scheme which is recovered, and enables one to recover not only differential-type schemes such as a particular SD method, but also integral-type schemes such as nodal DG schemes. However, whilst a general connection between FR and nodal DG schemes has been examined in other work [4, 9], there are many aspects of this equivalence that are yet to be investigated. A particularly important point that has so far remained widely unaddressed is that nodal DG schemes take on different numerical properties based on the choice of solution and quadrature points. We note that in a general nodal DG scheme, given an expansion on each element in terms of P Lagrange interpolants, we may perform quadrature on a separate set of Q quadrature points. If $P = Q$ and the distribution of solution and quadrature points is identical, then we recover the so-called discontinuous Galerkin spectral element method ($\mathrm{DG_{SEM}}$) which diagonalises the mass matrix, allowing for further computational optimisation [7, 15]. However, exactly which of these DG schemes can be recovered by the FR approach has not yet been examined.

The purpose of this paper is to examine connections between various DG and FR schemes for the case of an advection equation. We consider a nodal DG scheme with $Q > P$ and two $\mathrm{DG_{SEM}}$ schemes. In the following with the subscript SEM[†] we mean that a collocation quadrature rule is used for the inner product of the advection term of the conservation law equation.

Huynh in [4] proposed that one can recover a nodal DG scheme with the FR approach by using Radau polynomials for the correction functions. We refer to this FR scheme as $\mathrm{FR_{DG}}$. However, only the case of linear advection was investigated, hence aliasing issues arising from a nonlinear flux (which can lead to differences between the $\mathrm{FR_{DG}}$ and DG schemes) were not considered.
In this work we demonstrate that the $\mathrm{FR_{DG}}$ and DG schemes, on a regular grid, are also equivalent for a non-linear advection equation provided that a collocation quadrature rule is used for the the inner product of the advection term of the DG discretisation. In fact, by using this rule, the aliasing errors of the two schemes are identical. We perform a complete demonstration for the case of 2D advection equation on a quadrilateral regular grid (it can be easily extended to 3D regular grids).

[†]In [7, 15] the $\mathrm{DG_{SEM}}$ method implied a collocation quadrature rule for the inner product of all the terms of the discretisation and not only the advection term. This led to a diagonal mass matrix which, in the case of Gauss-Lobatto-Legendre points, is not an exact mass matrix but a lumped one.

DOI: 10.1002/fld

We state that this derivation is always valid on regular grids whilst some differences might exist on deformed girds. In the rest of the paper we will refer to this DG scheme as DG_{SEM} with exact mass matrix (second column of table I)). We observe that if an over-integration is used for the advection term the equivalence is valid only in the case of a linear flux function on a regular grid, since by over-integrating we are reducing the aliasing errors arising from the nonlinearities. Hereafter we will refer to this DG scheme as $DG_{Q>P}$ with exact mass matrix (third column of table I)).
Then we demonstrate, for the case of a 1D conservation law on a regular grid (the demonstration can be extended to 2D/3D regular tensor product grids), that a DG method with solution nodes collocated at Gauss-Lobatto-Legendre points recovers the FR g2 scheme introduced by Huynh in [4] when the mass matrix of the DG discretisation is lumped. The equivalence is valid for both the cases of a linear or nonlinear flux function provided that a collocation quadrature rule is used for the inner product of the advection term of the DG discretisation. In the following we refer to this DG sheme as DG_{SEM}-GLL with lumped mass matrix (first column of table I), and to the type of FR scheme recovered as FR_{g2} scheme. For the same reasons cited above, when an over-integration of the advection term is used the proof is valid only in the case of a linear flux function on a regular grid.
Experiments performed with both linear/nonlinear fluxes on regular/deformed grids using the spectral element framework Nektar++ confirm the connections between the different versions of nodal DG spectral element methods and the two types of FR schemes. Table I highlights the results of this study, and will be expanded upon further in the following section. We conclude with a brief study of the relative computational efficiencies of each scheme.

2. THEORY

In this section, we first describe the DG and FR methods in the setting of a 1D scalar conservation law and based on the arguments of Huynh [4], we prove the equality of DG_{SEM} and FR_{DG} schemes on a regular grid of quadrilateral elements. We further show that in one dimension the DG_{SEM}-GLL scheme is mathematically identical to the FR_{g2} scheme.

2.1. Discontinuous Galerkin method for 1D scalar conservation law

Consider the 1D scalar conservation law

$$\frac{\partial u}{\partial t} + \frac{\partial f}{\partial x} = 0 \tag{1}$$

within an domain $\Omega \subset \mathbb{R}$, where $f = f(u)$ is the flux function. The aim of the DG method is to find an approximate weak solution to Eq. 1 when the domain Ω is partitioned into N non-overlapping elements Ω_n such that

$$\Omega = \bigcup_{n=1}^{N} \Omega_n.$$

From an implementation perspective, it is convenient to map each element Ω_n into a reference (standard) element $\Omega_s = \{\xi \mid -1 \leq \xi \leq 1\}$ where

$$x = \Theta_n(\xi) = \left(\frac{1-\xi}{2}\right) x_n + \left(\frac{1+\xi}{2}\right) x_{n+1}.$$

In the reference domain the transformed equation into Ω_s becomes

$$\frac{\partial \hat{u}_n^\delta}{\partial t} + \frac{\partial \hat{f}_n^\delta}{\partial \xi} = 0,$$

where

$$\hat{u}_n^\delta = \hat{u}_n^\delta(\xi, t) = u_n^\delta(\Theta_n^{-1}(\xi), t),$$

DOI: 10.1002/fld

$$\hat{f}_n^\delta = \hat{f}_n^\delta(\xi,t) = \frac{f_n^\delta(\Theta_n^{-1}(\xi),t)}{J_n},$$

with $J_n = (x_{n+1} - x_n)/2$. The transformed solution $\hat{u}_n^\delta$ in the reference space is approximated by a polynomial of degree P and can be written as

$$\hat{u}_n^\delta = \sum_{i=0}^{P} \hat{u}_i^\delta \ell_i(\xi), \tag{2}$$

where ℓ_i denote the Lagrange polynomials. Analogously the approximate transformed flux $\hat{f}_n^\delta$ in the reference space can be written as

$$\hat{f}_n^{\delta D} = \sum_{i=0}^{P} \hat{f}_i^{\delta D} \ell_i(\xi). \tag{3}$$

Here the superscript D stands for discontinuous since the flux is calculated directly from the approximate solution, which is in general piecewise discontinuous between elements.

Now, we write the residual of Eq. 2.1

$$R^\delta = \frac{\partial \hat{u}_n^\delta}{\partial t} + \frac{\partial \hat{f}_n^\delta}{\partial \xi}$$

which we require to be orthogonal to a set of smooth test functions. Following the standard Galerkin approach we choose test functions defined by the basis $\ell_i(\xi)$ leading to the condition that

$$\int_{\Omega_s} R^\delta \cdot \ell_i \, d\xi \qquad \forall\, i.$$

After performing integration by parts, substituting the boundary terms by the numerical interface fluxes and integrating by parts once more we derive the strong form of the DG method,

$$\frac{\partial}{\partial t}\int_{\Omega_s} \hat{u}_n^\delta(\xi)\cdot\ell_i(\xi)\,d\xi \; + \int_{\Omega_s} \frac{\partial}{\partial \xi}\hat{f}_n^{\delta D}(\xi)\cdot\ell_i(\xi)\,d\xi \; + \left[\left(\hat{f}_n^{\delta I} - \hat{f}_n^{\delta D}\right)\cdot\ell_i(\xi)\right]_{-1}^{+1} = 0 \qquad \forall\, i. \tag{4}$$

The $P+1$ equations can be written in matrix form as

$$\mathbf{M}\frac{d\hat{\mathbf{u}}_n^\delta}{dt} + \mathbf{S}\hat{\mathbf{f}}_n^{\delta D} = \left[\left(\hat{f}_n^{\delta D} - \hat{f}_n^{\delta I}\right)\mathbf{l}(\xi)\right]_{-1}^{+1} \tag{5}$$

where $\mathbf{M}$ and $\mathbf{S}$ are the local mass matrix and stiffness matrices

$$M_{i,j} = \int_{\Omega_s} \ell_i(\xi)\ell_j(\xi)\,d\xi, \qquad S_{i,j} = \int_{\Omega_s} \ell_i(\xi)\frac{d\ell_j(\xi)}{d\xi}\,d\xi, \tag{6}$$

and $\mathbf{l}(\xi) = [\ell_0(\xi), ..., \ell_P(\xi)]$.

2.2. *Flux reconstruction method for 1D scalar conservation law*

After having obtained the formulation of DG scheme for the 1D scalar equation on a regular grid, we follow the approach of Huynh [4] to write the formulation of the FR scheme.

Consider again the 1D scalar conservation law of Eq. 1. As before, we discretize the domain into N non-overlapping standard elements and we map each of them into a standard element Ω_s. The solution $\hat{u}_n^\delta$ in the reference space can again be expanded in a polynomial basis as in Eq. 2. The approximate flux in the standard element can be written as

$$\hat{f}_n^\delta = \hat{f}_n^\delta(\xi,t) = \hat{f}_n^{\delta D} + \hat{f}_n^{\delta C}$$

where $\hat{f}_n^{\delta D}$ remains defined as in Eq. 3 and

$$\hat{f}_n^{\delta C} = h_L(\xi)\left[\hat{f}_n^{\delta I} - \hat{f}_n^{\delta D}\right]\Big|_{\xi=-1} + \quad h_R(\xi)\left[\hat{f}_n^{\delta I} - \hat{f}_n^{\delta D}\right]\Big|_{\xi=1} = \widehat{\Delta f}_L h_L + \widehat{\Delta f}_R h_R.$$

DOI: 10.1002/fld

In the above, D stands for discontinuous, C stands for corrective, $\widehat{\Delta f}_L$ and $\widehat{\Delta f}_R$ are the left and right jump fluxes at the boundary, $h_L(\xi)$ and $h_R(\xi)$ are the left and right correction functions which have to approximate zero in some sense and satisfy

$$h_L(-1) = 1, \quad h_L(1) = 0, \quad h_R(-1) = 0, \quad h_R(1) = 1.$$

The derivative of the flux with respect to ξ is

$$\frac{\partial \hat{f}_n^\delta}{\partial \xi} = \frac{\partial \hat{f}_n^{\delta D}}{\partial \xi} + \frac{\partial \hat{f}_n^{\delta C}}{\partial \xi} = \frac{\partial \hat{f}_n^{\delta D}}{\partial \xi} + \widehat{\Delta f}_L \frac{dh_L}{\partial \xi} + \widehat{\Delta f}_R \frac{dh_R}{\partial \xi}$$

As noted by Jameson et al. [14] the functions $h_L(\xi)$ and $h_R(\xi)$ can be defined in the space of polynomials of degree at most $P+1$. As a consequence the derivatives $\frac{dh_L}{\partial \xi}$ and $\frac{dh_R}{\partial \xi}$ can be represented in the same basis as the solution $\hat{u}_n^\delta$. This gives the formulation of the FR scheme:

$$\frac{\partial \hat{u}_n^\delta}{\partial t} + \frac{\partial \hat{f}_n^{\delta D}}{\partial \xi} + \widehat{\Delta f_L} \frac{dh_L}{\partial \xi} + \widehat{\Delta f_R} \frac{dh_R}{\partial \xi} = 0. \tag{7}$$

Now, we require the residual of Eq. 7 to be orthogonal to a set of smooth function as before and we therefore obtain

$$\begin{aligned} &\frac{\partial}{\partial t} \int_{\Omega_s} \hat{u}_n^\delta(\xi) \cdot \ell_i(\xi)\, d\xi \; + \int_{\Omega_s} \frac{\partial}{\partial \xi} \hat{f}_n^{\delta D}(\xi) \cdot \ell_i(\xi)\, d\xi \; + \\ &\int_{\Omega_s} \left(\widehat{\Delta f_L} h_L'(\xi) + \widehat{\Delta f_R} h_R'(\xi) \right) \cdot \ell_i(\xi)\, d\xi \;\; = 0 \quad \forall i. \end{aligned}$$

Performing an integration by parts on the last term we see that

$$\begin{aligned} &\frac{\partial}{\partial t} \int_{\Omega_s} \hat{u}_n^\delta(\xi) \cdot \ell_i(\xi)\, d\xi \; + \int_{\Omega_s} \frac{\partial}{\partial \xi} \hat{f}_n^{\delta D}(\xi) \cdot \ell_i(\xi)\, d\xi \; + \\ &\widehat{\Delta f_L} \cdot \ell_i(-1) - \widehat{\Delta f_R} \cdot \ell_i(1) - \\ &\int_{\Omega_s} \left(\widehat{\Delta f_L} h_L(\xi) + \widehat{\Delta f_R} h_R(\xi) \right) \cdot \ell_i'(\xi)\, d\xi \;\; = 0 \quad \forall i. \end{aligned} \tag{8}$$

and so eq. 8 becomes

$$\begin{aligned} &\frac{\partial}{\partial t} \int_{\Omega_s} \hat{u}_n^\delta(\xi) \cdot \ell_i(\xi)\, d\xi \; + \int_{\Omega_s} \frac{\partial}{\partial \xi} \hat{f}_n^{\delta D}(\xi) \cdot \ell_i(\xi)\, d\xi \; + \left[\left(\hat{f}_n^{\delta I} - \hat{f}_n^{\delta D} \right) \cdot \ell_i(\xi) \right]_{-1}^{+1} - \\ &\int_{\Omega_s} \left(\widehat{\Delta f_L} h_L(\xi) + \widehat{\Delta f_R} h_R(\xi) \right) \cdot \ell_i'(\xi) \;\; = 0 \quad \forall i. \end{aligned} \tag{9}$$

Eq. 9 is equal to Eq. 4 except for the last term. As pointed out by Huynh in in [4], that term vanishes if we define h_L and h_R using Radau polynomials of order $P+1$ because a Radau polynomial of order $P+1$ is orthogonal to all the polynomials of order less than or equal to $P-1$. Therefore, we recover exactly the DG method, at least for the case of a linear flux function. We refer to this type of FR scheme with correction functions equal to Radau polynomials as FR_{DG}.

The $P+1$ equations can be written in matrix form as:

$$\frac{d\hat{\mathbf{u}}_n^\delta}{dt} + \mathbf{D}\hat{\mathbf{f}}_n^{\delta D} + \widehat{\Delta f}_L \mathbf{h}_L(\xi) + \widehat{\Delta f}_R \mathbf{h}_R(\xi) = 0$$

where $\mathbf{D} = \mathbf{M}^{-1}\mathbf{S}$ is the local differentiation matrix with $D_{i,j} = l_j'(\xi_i)$, $\mathbf{h}_L'(\xi) = [h_L'(\xi_0), ..., h_L'(\xi_P)]$ and $\mathbf{h}_R'(\xi) = [h_R'(\xi_0), ..., h_R'(\xi_P)]$.

DOI: 10.1002/fld

2.3. 2D scalar conservation law on quadrilateral grids

In this subsection we demonstrate the equality of DG and FR_{DG} on meshes of regular quadrilateral elements. Consider the 2D scalar conservation law

$$\frac{\partial u}{\partial t} + \nabla_{xy} \cdot \mathbf{f} = 0$$

within a domain $\Omega \subset \mathbb{R}^2$, with $\mathbf{f} = (f, g)$, where $f = f(u)$ and $g = g(u)$ are the fluxes in the x and y directions respectively. The domain Ω is partitioned into N non-overlapping, conforming quadrilateral elements Ω_n such that

$$\Omega = \bigcup_{n=1}^{N} \Omega_n.$$

As in the one dimensional case, we map each quadrilateral element Ω_n into a reference element $\Omega_s = [-1, 1]^2$ in the transformed space $\widehat{\boldsymbol{x}} = (\xi, \eta)$ so that

$$\boldsymbol{x} = \Theta_n(\widehat{\boldsymbol{x}}) = \sum_{i=1}^{K} \boldsymbol{M}_i \boldsymbol{x}_{i,n}. \tag{10}$$

Here $\boldsymbol{M}_i$ are the transformation functions, $\boldsymbol{x}_{i,n}$ are the physical coordinates of the points which describe each physical element Ω_n and K is the number of points. In the reference domain the transformed equation into any individual Ω_s becomes

$$\frac{\partial \hat{u}_n^\delta}{\partial t} + \nabla_{\xi\eta} \cdot \hat{\mathbf{f}}_n^\delta = 0, \tag{11}$$

where

$$\hat{u}_n^\delta = \hat{u}_n^\delta(\xi, \eta, t) = J_n u_n^\delta(\Theta^{-1}(\xi, \eta), t),$$

$$\hat{\mathbf{f}}_n^\delta = \hat{\mathbf{f}}_n^\delta(\xi, \eta, t) = (\hat{f}_n^\delta, \hat{g}_n^\delta) = \left(\frac{\partial y}{\partial \eta} f_n^\delta - \frac{\partial x}{\partial \eta} g_n^\delta, -\frac{\partial y}{\partial \xi} f_n^\delta + \frac{\partial x}{\partial \xi} g_n^\delta \right),$$

and the metric terms J_n, $\frac{\partial x}{\partial \xi}$, $\frac{\partial x}{\partial \eta}$, $\frac{\partial y}{\partial \xi}$, $\frac{\partial y}{\partial \eta}$ can be evaluated from Eq. 10. The transformed solution $\hat{u}_n^\delta$ in the reference space within each element is approximated by a polynomial of degree P and can be written as

$$\hat{u}_n^\delta = \sum_{i,j=0}^{i,j=P} \hat{u}_{i,j}^\delta \ell_{i,j}(\xi, \eta) = \sum_{i,j=0}^{i,j=P} \hat{u}_{i,j}^\delta \ell_i(\xi) \ell_j(\eta), \tag{12}$$

where $\ell_i(\xi)$ and $\ell_j(\eta)$ are one-dimensional Lagrange polynomials of order P of the nodal basis associated with the 1D solution points along ξ and η directions. The polynomial $\ell_{i,j}(\xi, \eta)$ is obtained by the tensor product of the 1D nodal bases $\ell_i(\xi)$ and $\ell_j(\eta)$ such that

$$\ell_{i,j}(\xi_l, \eta_m) = \begin{cases} 1, & \text{if } (\xi_l, \eta_m) = (\xi_i, \eta_j), \\ 0, & \text{if } (\xi_l, \eta_m) \neq (\xi_i, \eta_j). \end{cases} \tag{13}$$

Analogously the approximate transformed fluxes $\hat{f}_n^{\delta D}$ and $\hat{g}_n^{\delta D}$ in the reference space within each element can be written as

$$\hat{f}_n^{\delta D} = \sum_{i,j=0}^{i,j=P} \hat{f}_{i,j}^{\delta D} \ell_{i,j}(\xi, \eta) = \sum_{i,j=0}^{i,j=P} \hat{f}_{i,j}^{\delta D} \ell_i(\xi) \ell_j(\eta), \tag{14}$$

$$\hat{g}_n^{\delta D} = \sum_{i,j=0}^{i,j=P} \hat{g}_{i,j}^{\delta D} \ell_{i,j}(\xi, \eta) = \sum_{i,j=0}^{i,j=P} \hat{g}_{i,j}^{\delta D} \ell_i(\xi) \ell_j(\eta), \tag{15}$$

DOI: 10.1002/fld

where the superscript D again stands for discontinuous since the fluxes are calculated directly from the approximate solution, which is in general piecewise discontinuous between elements.

To prove that the DG method is identical to FR_{DG} for the case of a 2D scalar equation we first write the residual of Eq. 11 as

$$R^{\delta} = \frac{\partial \hat{u}_n^{\delta}}{\partial t} + \frac{\partial \hat{f}_n^{\delta}}{\partial \xi} + \frac{\partial \hat{g}_n^{\delta}}{\partial \eta},$$

and we require the residual R^{δ} to be orthogonal to a set of smooth test functions. The use of test functions defined by the basis $\ell_{i,j}(\xi,\eta)$ leads to the following equation:

$$\iint_{\Omega_s} R^{\delta} \cdot \ell_{i,j} \, d\xi d\eta = 0 \qquad \forall\, i,j.$$

Performing the integration by parts, substituting the boundary terms by the numerical interface fluxes and integrating by parts once more we derive the strong form of the DG method,

$$\begin{aligned}
&\frac{\partial}{\partial t} \iint_{\Omega_s} \hat{u}_n^{\delta}(\xi,\eta) \cdot \ell_{i,j}(\xi,\eta) \; d\xi \, d\eta + \\
&\iint_{\Omega_s} \frac{\partial}{\partial \xi} \hat{f}_n^{\delta D}(\xi,\eta) \cdot \ell_{i,j}(\xi,\eta) \; d\xi \, d\eta \; + \iint_{\Omega_s} \frac{\partial}{\partial \eta} \hat{g}_n^{\delta D}(\xi,\eta) \cdot \ell_{i,j}(\xi,\eta) \; d\xi \, d\eta + \\
&\int_{-1}^{1} \left[\hat{f}_n^{\delta I}(1,\eta) - \hat{f}_n^{\delta D}(1,\eta) \right] \cdot \ell_{i,j}(1,\eta) \; d\eta \; - \int_{-1}^{1} \left[\hat{f}_n^{\delta I}(-1,\eta) - \hat{f}_n^{\delta D}(-1,\eta) \right] \cdot \ell_{i,j}(-1,\eta) \; d\eta + \\
&\int_{-1}^{1} \left[\hat{g}_n^{\delta I}(\xi,1) - \hat{g}_n^{\delta D}(\xi,1) \right] \cdot \ell_{i,j}(\xi,1) \; d\xi \; - \int_{-1}^{1} \left[\hat{g}_n^{\delta I}(\xi,-1) - \hat{g}_n^{\delta D}(\xi,-1) \right] \cdot \ell_{i,j}(\xi,-1) \; d\xi = 0, \\
&\forall\, i,j.
\end{aligned}$$

Via the tensor product the above equation can be rewritten as:

$$\begin{aligned}
&\frac{\partial}{\partial t} \iint_{\Omega_s} \hat{u}_n^{\delta}(\xi,\eta) \cdot \ell_{i,j}(\xi,\eta) \; d\xi \, d\eta + \\
&\iint_{\Omega_s} \frac{\partial}{\partial \xi} \hat{f}_n^{\delta D}(\xi,\eta) \cdot \ell_{i,j}(\xi,\eta) \; d\xi \, d\eta \; + \iint_{\Omega_s} \frac{\partial}{\partial \eta} \hat{g}_n^{\delta D}(\xi,\eta) \cdot \ell_{i,j}(\xi,\eta) \; d\xi \, d\eta + \\
&\int_{-1}^{1} \left[\hat{f}_n^{\delta I}(1,\eta) - \hat{f}_n^{\delta D}(1,\eta) \right] \cdot \ell_i(1)\ell_j(\eta) \; d\eta \; - \int_{-1}^{1} \left[\hat{f}_n^{\delta I}(-1,\eta) - \hat{f}_n^{\delta D}(-1,\eta) \right] \cdot \ell_i(-1)\ell_j(\eta) \; d\eta + \\
&\int_{-1}^{1} \left[\hat{g}_n^{\delta I}(\xi,1) - \hat{g}_n^{\delta D}(\xi,1) \right] \cdot \ell_i(\xi)\ell_j(1) \; d\xi \; - \int_{-1}^{1} \left[\hat{g}_n^{\delta I}(\xi,-1) - \hat{g}_n^{\delta D}(\xi,-1) \right] \cdot \ell_i(\xi)\ell_j(-1) \; d\xi = 0, \\
&\forall\, i,j
\end{aligned} \tag{16}$$

As shown by Huynh in [4], we can write $\ell(-1)$ through the expression

$$\int_{-1}^{1} h'_L(\xi)\ell(\xi) \; d\xi = \int_{-1}^{1} h'_B(\eta)\ell(\eta) \; d\eta = -\ell(-1), \tag{17}$$

where L and B denote left and bottom edges respectively, $h_L(\xi)$ and $h_B(\eta)$ are the right Radau polynomials of order $P+1$ on $[-1,1]$ which vanish at the right boundary $\xi = \eta = 1$. This is due to the orthogonality of the right Radau polynomial of order $P+1$ to all polynomials of order up to $P-1$. Analogously, we can write $\ell(1)$ using the expression

$$\int_{-1}^{1} h'_R(\xi)\ell(\xi) \; d\xi = \int_{-1}^{1} h'_T(\eta)\ell(\eta) \; d\eta = \ell(1), \tag{18}$$

DOI: 10.1002/fld

where R and T denote right and top edges and $h_R(\xi)$ and $h_T(\eta)$ are the left Radau polynomials of order $P+1$ on $[-1,1]$ which vanish at the left boundary $\xi=\eta=-1$.

Substituting Eqs. 17 and 18 into Eq. 16 leads to

$$\frac{\partial}{\partial t}\iint_{\Omega_s}\hat{u}_n^{\delta}(\xi,\eta)\cdot\ell_{i,j}(\xi,\eta)\,d\xi\,d\eta+$$
$$\iint_{\Omega_s}\left\{\hat{f}_n^{\delta D}(\xi,\eta)+\left[\hat{f}_n^{\delta I}(1,\eta)-\hat{f}_n^{\delta D}(1,\eta)\right]h_R(\xi)+\left[\hat{f}_n^{\delta I}(-1,\eta)-\hat{f}_n^{\delta D}(-1,\eta)\right]h_L(\xi)\right\}_{/\xi}\cdot\ell_i(\xi)\ell_j(\eta)\,d\eta+$$
$$\iint_{\Omega_s}\left\{\hat{g}_n^{\delta D}(\xi,\eta)+\left[\hat{g}_n^{\delta I}(\xi,1)-\hat{g}_n^{\delta D}(\xi,1)\right]h_T(\eta)+\left[\hat{g}_n^{\delta I}(\xi,-1)-\hat{g}_n^{\delta D}(\xi,-1)\right]h_B(\eta)\right\}_{/\eta}\cdot\ell_i(\xi)\ell_j(\eta)\,d\eta=0,$$
$$\forall\, i,j.$$

Finally, by defining the fluxes $F_n^{\delta}(\xi,\eta)$ and $G_n^{\delta}(\xi,\eta)$ to be

$$\begin{cases}F_n^{\delta}(\xi,\eta)=\hat{f}_n^{\delta D}(\xi,\eta)+\left[\hat{f}_n^{\delta I}(1,\eta)-\hat{f}_n^{\delta D}(1,\eta)\right]h_R(\xi)+\left[\hat{f}_n^{\delta I}(-1,\eta)-\hat{f}_n^{\delta D}(-1,\eta)\right]h_L(\xi)\\ G_n^{\delta}(\xi,\eta)=\hat{g}_n^{\delta D}(\xi,\eta)+\left[\hat{g}_n^{\delta I}(\xi,1)-\hat{g}_n^{\delta D}(\xi,1)\right]h_T(\eta)+\left[\hat{g}_n^{\delta I}(\xi,-1)-\hat{g}_n^{\delta D}(\xi,-1)\right]h_B(\eta)\end{cases}$$

we can write

$$\iint_{\Omega_s}\left\{\left(\hat{u}_n^{\delta}(\xi,\eta)\right)_{/t}+\left(F_n^{\delta}(\xi,\eta)\right)_{/\xi}+\left(G_n^{\delta}(\xi,\eta)\right)_{/\eta}\right\}\cdot\ell_{i,j}(\xi,\eta)\,d\xi\,d\eta=0. \tag{19}$$

Since $\hat{u}_n^{\delta}(\xi,\eta)$, $\left(F_n^{\delta}(\xi,\eta)\right)_{/\xi}$ and $\left(G_n^{\delta}(\xi,\eta)\right)_{/\eta}$ are polynomials of degree P and Eq. 19 is valid for any polynomial $\ell_{i,j}(\xi,\eta)$ of degree P we can eliminate the integrals and write:

$$\left(\hat{u}_n^{\delta}(\xi,\eta)\right)_{/t}+\left(F_n^{\delta}(\xi,\eta)\right)_{/\xi}+\left(G_n^{\delta}(\xi,\eta)\right)_{/\eta}=0. \tag{20}$$

This proves that the FR approach recovers the DG method, at least for the case of a linear flux function on a tensor-product grid, when Radau polynomials are used as correction functions leading to the FR_{DG} scheme.

By using Eqs. 12, 13, 14 and 15 the equation for the generic point (ξ_i,η_j) becomes:

$$\begin{aligned}\frac{d\hat{u}_{i,j}}{dt}=&-\left.\frac{\partial\hat{f}_n^{\delta D}}{\partial\xi}\right|_{\xi_i,\eta_j}-\left.\frac{\partial\hat{g}_n^{\delta D}}{\partial\eta}\right|_{\xi_i,\eta_j}\\ &-\left[\hat{f}_n^{\delta I}(1,\eta_j)-\hat{f}_n^{\delta D}(1,\eta_j)\right]\left.\frac{\partial h_R}{\partial\xi}\right|_{\xi_i}-\left[\hat{f}_n^{\delta I}(-1,\eta_j)-\hat{f}_n^{\delta D}(-1,\eta_j)\right]\left.\frac{\partial h_L}{\partial\xi}\right|_{\xi_i}\\ &-\left[\hat{g}_n^{\delta I}(\xi_i,1)-\hat{g}_n^{\delta D}(\xi_i,1)\right]\left.\frac{\partial h_T}{\partial\eta}\right|_{\eta_j}-\left[\hat{g}_n^{\delta I}(\xi_i,-1)-\hat{g}_n^{\delta D}(\xi_i,-1)\right]\left.\frac{\partial h_B}{\partial\eta}\right|_{\eta_j}.\end{aligned} \tag{21}$$

2.4. *FR_{g2} as DG_{SEM}-GLL with lumped mass matrix*

In [14] it was shown that some linearly filtered DG methods can be expressed in the flux reconstruction framework. Equivalently, some FR schemes can be described as a DG method for which a linear filtering operator is applied on the residual. In particular the entire class of energy-stable FR schemes introduced by Vincent et al. in [9] can be recast as a filtered DG method. In this subsection we demonstrate the equivalence between the Huynh's g2 FR scheme and a particular type of filtered DG scheme.

For Eq. 2.1 the classical DG method can be written as

$$\mathbf{M}\frac{d\hat{\mathbf{u}}_n^{\delta}}{dt}+\mathbf{S}\hat{\mathbf{f}}_n^{\delta D}=\left[\left(\hat{f}_n^{\delta D}-\hat{f}_n^{\delta I}\right)\mathbf{l}(\xi)\right]_{-1}^{+1} \tag{22}$$

DOI: 10.1002/fld

where $\mathbf{M}$ and $\mathbf{S}$ again denote the local mass and stiffness matrices. The filtered DG method is

$$\widetilde{\mathbf{M}}\frac{d\hat{\mathbf{u}}_n^\delta}{dt} - \mathbf{S}\hat{\mathbf{f}}_n^{\delta D} = \left[\hat{f}_n^{\delta I}\mathbf{l}(\xi)\right]_{-1}^{+1}$$

where

$$\widetilde{\mathbf{M}} = \mathbf{M}\cdot\mathbf{F}^{-1} \tag{23}$$

and $\mathbf{F}$ denotes a linear filter. For Huynh's g2 FR scheme the explicit form of the filter in the non-normalized Legendre basis is a diagonal matrix of the form

$$\mathbf{F_P} = \begin{bmatrix} 1 & & & \\ & \ddots & & \\ & & 1 & \\ & & & \frac{P}{1+\frac{2P+1}{2}(P!a_P)^2} \end{bmatrix},$$

where

$$a_P = \frac{(2P)!}{2^P(P!)^2}.$$

The filter can be transformed to the computational basis B so that

$$\mathbf{F_B} = {\mathbf{V_{B,P}}}^{-1}\cdot\mathbf{F_P}\cdot\mathbf{V_{B,P}}, \tag{24}$$

where $\mathbf{V_{B,P}}$ is the transformation matrix from a general and unspecified basis B to basis P. If we consider a basis B which represents the solution $\hat{u}_n^\delta$ in terms of Lagrange polynomials with solution values at $P+1$ Gauss-Lobatto-Legendre (GLL) points, substituting Eq. 24 in Eq. 23 we obtain

$$\widetilde{\mathbf{M}} = \begin{bmatrix} \ddots & & \\ & w_i & \\ & & \ddots \end{bmatrix} \tag{25}$$

where w_i denote the weights of the GLL quadrature rule at the $P+1$ points.

Consider now Eq. 22 with solution coefficients $\hat{u}_n^\delta$ represented by Lagrange polynomials with solution values at $P+1$ GLL points. If we additionally choose a GLL quadrature to utilise a $\mathrm{DG_{SEM}}$ scheme, then as it is well known that this rule is exact only for polynomials up to order $2P-1$, the coefficients of the mass matrices as defined in Eq. 6 will contain a numerical quadrature error since each integrand is a polynomial of order $2P$. However, since the Lagrangian basis has the property that $\ell_i(\xi_j) = \delta_{ij}$ where δ_{ij} represents the Kronecker delta function, with this quadrature rule the mass matrix $\mathbf{M}$ obtained is diagonal,

$$\mathbf{M} = \begin{bmatrix} \ddots & & \\ & w_i & \\ & & \ddots \end{bmatrix} \tag{26}$$

where w_i are the weights of the GLL quadrature rule. This renders the scheme extremely efficient as the mass matrix is now trivially invertible.

The mass matrix of Eq. 26 is equal to that of Eq. 25, so Huynh's g2 FR scheme can be seen as a DG scheme where mass matrix $\mathbf{M}$ is lumped. We refer to this type of DG scheme as $\mathrm{DG_{SEM}}$-GLL with lumped mass matrix and the type of FR scheme recovered as $\mathrm{FR_{g2}}$. Therefore, in this case we recover exactly the $\mathrm{DG_{SEM}}$-GLL with lumped mass matrix method at least for the case of a linear flux function.

DOI: 10.1002/fld

2.5. Summary

In the previous sections we have derived the connections between the DG method and FR schemes in the case of an advection problem. A summary of the results of this section can be seen in table I, where the connections between the three DG and two FR schemes is presented.

In the first two columns of the table we consider two nodal types of DG_{SEM} scheme.
The DG_{SEM} method with exact mass matrix is equivalent to the FR_{DG} scheme.
The DG_{SEM}-GLL (solution values at Gauss-Lobatto-Legendre points) method with lumped mass matrix is equivalent to the FR_{g2} scheme.
The equivalences are valid both for linear and nonlinear flux functions.

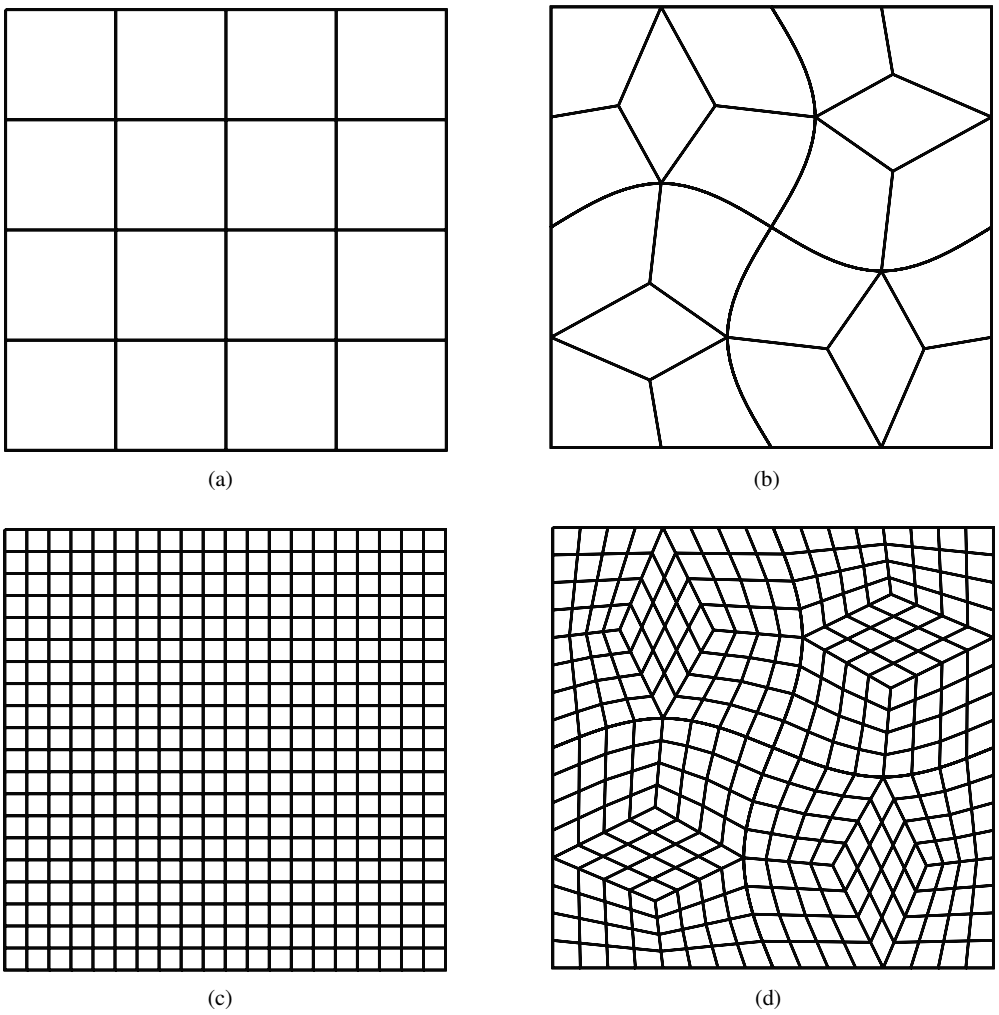

Figure 1. Meshes utilised in the numerical experiments. The grids on the left are regular and on the right are deformed.

In the third column of this table we consider an arbitrary nodal DG scheme and state that Q (the quadrature order) must be larger than P (the polynomial order). We note that this statement does not necessarily means that the number of quadrature points is higher than the number of solution points but only that the precision of the quadrature rule chosen is higher than that of a collocation quadrature rule. For example, if the solution values are at P Gauss-Lobatto-Legdendre (GLL)

DOI: 10.1002/fld

points and the quadrature points are at Q Gauss-Legendre (GL) points with $Q = P$, the quadrature precision is higher than that obtained with the same number of quadrature points collocated at GLL points. We additionally note that the $\mathrm{DG}_{\mathrm{Q>P}}$ scheme with exact mass matrix and is equivalent to the $\mathrm{FR}_{\mathrm{DG}}$ scheme when the flux function is linear. If the flux function is nonlinear the schemes are different because the the aliasing errors arising from the nonlinearities are minimised in the DG scheme by using a quadrature with a higher precision.

All of the derivations above assume that the elemental Jacobian is constant in space, so that each element is not deformed. In the case of a deformed grid it is not ensured that the results are always valid. The deformation of the grid introduces a nonlinearity in the equations and, then, the equivalences depend on the approximation of the geometric factors.

3. NUMERICAL EXPERIMENTS

A range of numerical experiments were undertaken in order to confirm the theoretical equality of the schemes as proven in the previous section. These simulations take into consideration both linear and nonlinear flux functions. Four grids were generated of the same domain $\Omega = [0, 10] \times [-5, 5]$, as shown in figure 1. The first of these (figure 1(a)) is a structured subdivision of the domain into a 4×4 array of regular quadrilaterals (i.e. the Jacobian is constant across each element). To demonstrate the schemes' equivalence for curvilinear (i.e. spatially varying Jacobian), an additional unstructured grid has been generated as shown in figure 1(b). These meshes were used for simulations of the linear flux function which will be presented below. Additionally the grids depicted in figures 1(c) and 1(d), which possess 400 and 320 elements respectively, were obtained through subdivision of these meshes and were used for simulations of the nonlinear flux functions.

3.1. Linear flux

This series of experiments were undertaken on the 2D linear advection equation:

$$\frac{\partial u}{\partial t} + \mathbf{a} \cdot \nabla u = 0, \qquad \mathbf{a} = [1, 0]. \tag{27}$$

The solution was represented by a fifth, seventh, ninth and eleventh order polynomial. First the polynomials were defined by a collocation projection of the solution values at six, eight, ten and twelve GLL points for each element. Then the calculations were repeated using GL points. In all the cases a collocation quadrature rule was used for the inner product of the advection term of the DG scheme. With GLL points both the cases of exact mass matrix (EMM) and and lumped mass matrix (LMM) were considered. Periodic conditions were applied at the boundary of the grids, and the Gaussian profile

$$u(x, y, 0) = e^{-40(x^2+y^2)}. \tag{28}$$

was used as an initial condition at $t = 0$. A fourth-order explicit Runge-Kutta time integration scheme was used to discretize the equations in time. The final time of the simulation was fixed at $T = 2s$ so that the exact solution is equal to the initial condition of Eq. 28. The time step was chosen to be sufficiently small so as to consider the temporal error negligible.

As the theoretical results suggest, figure 2(a) confirms that for regular elements the L^2 error of the final solution field for each DG scheme in table I precisely matches the equivalent FR scheme. Figure 2(b) also shows that the results match on the deformed grid because the approximation of the geometric factors is performed in the same way for both approaches. For both regular and deformed grids the results are identical up to machine precision. In figure 3 we see that the solution at the final time on the regular grid and on the deformed grid also correlate.

DOI: 10.1002/fld

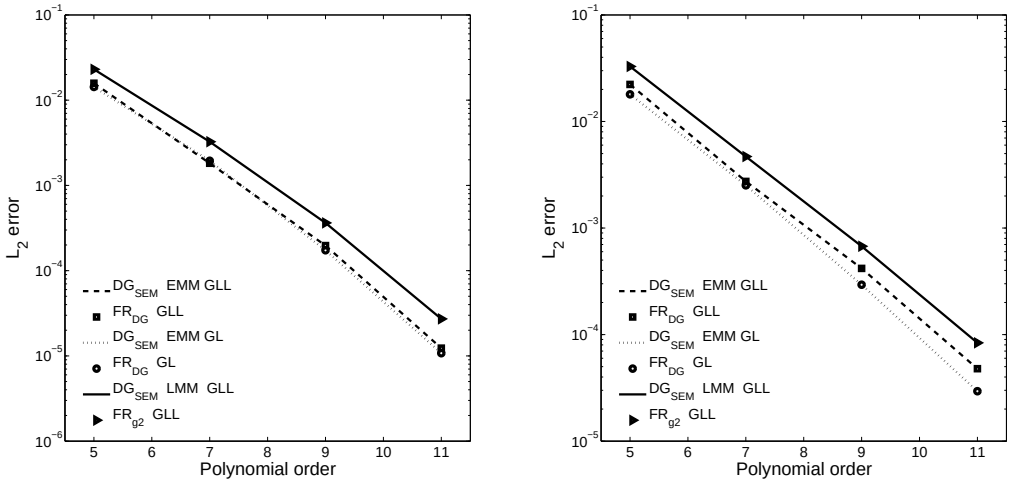

(a) (b)

Figure 2. L^2 error of the final solution vs. polynomial order P. On the left the results on the regular grid. On the right the results on the deformed grid. Results from the DG simulations are indicated by lines, whereas results from FR simulations are indicated by markers.

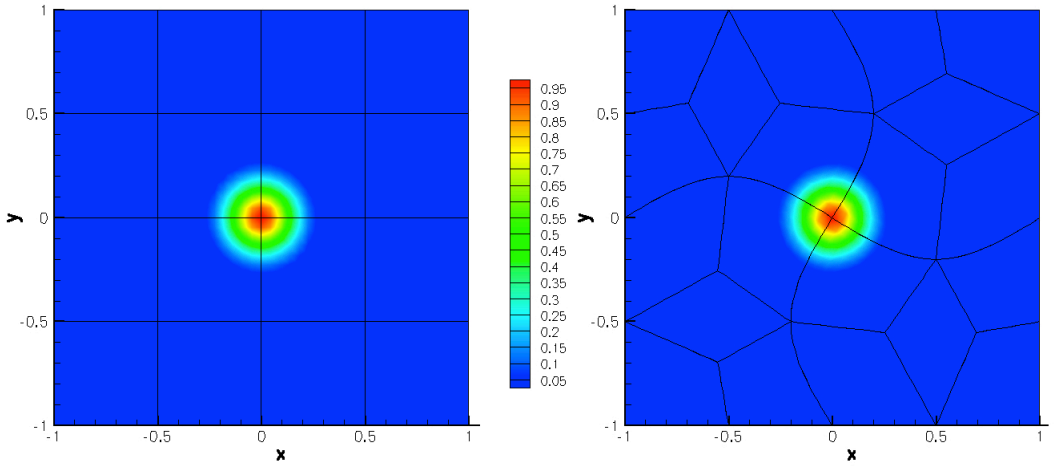

Figure 3. Visualization of the solution field at the final time $T = 2s$. On the left we depict the regular grid with solution values at twelve Gauss-Legendre points. On the right the deformed grid with solution values at twelve Gauss-Lobatto-Legendre points is shown.

3.2. Nonlinear flux

This series of experiments were undertaken using the two-dimensional Euler equations which govern the flow of a compressible inviscid fluid. These can be written as

$$\frac{\partial \mathbf{q}}{\partial t} + \frac{\partial \mathbf{F}^i}{\partial x} + \frac{\partial \mathbf{G}^i}{\partial y} = 0,$$

DOI: 10.1002/fld

where $\mathbf{q} = (\rho, \rho u, \rho v, E)^\top$ is the vector of the conserved variables and $\mathbf{F}^i = \mathbf{F}^i(\mathbf{q})$ and $\mathbf{G}^i = \mathbf{G}^i(\mathbf{q})$ are the vectors of the inviscid fluxes,

$$\mathbf{F}^i = \left\{ \begin{array}{c} \rho u \\ p + \rho u^2 \\ \rho uv \\ u(E+p) \end{array} \right\}, \qquad \mathbf{G}^i = \left\{ \begin{array}{c} \rho v \\ \rho uv \\ p + \rho v^2 \\ v(E+p) \end{array} \right\}. \tag{29}$$

In the above, ρ is the density, u and v are the velocity components in x and y directions, p is the pressure and E is the total energy.

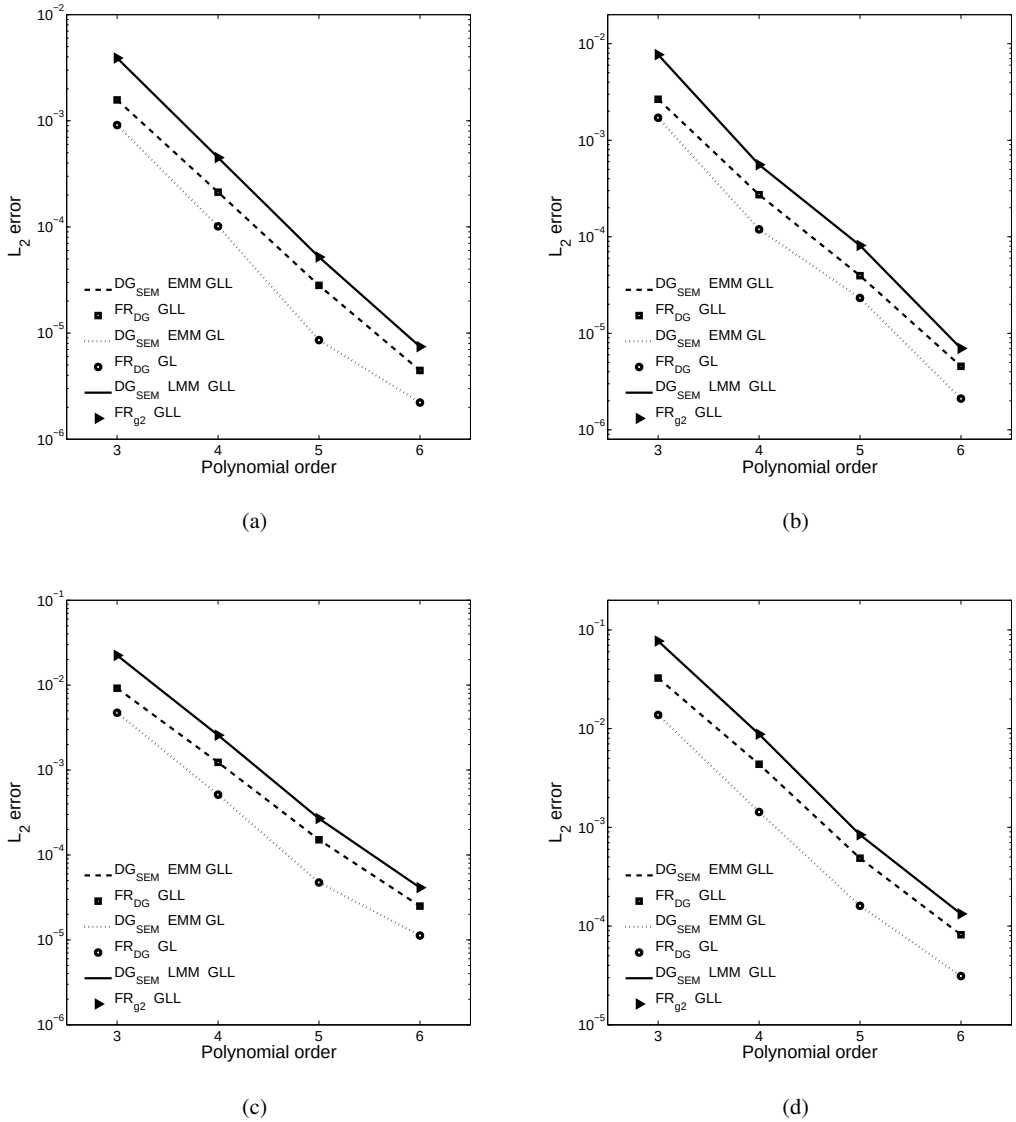

Figure 4. L^2 error vs polynomial order P on the regular grid at the final time $T = 2s$. Figures (a)-(d) depict ρ, ρu, ρv and E respectively.

DOI: 10.1002/fld

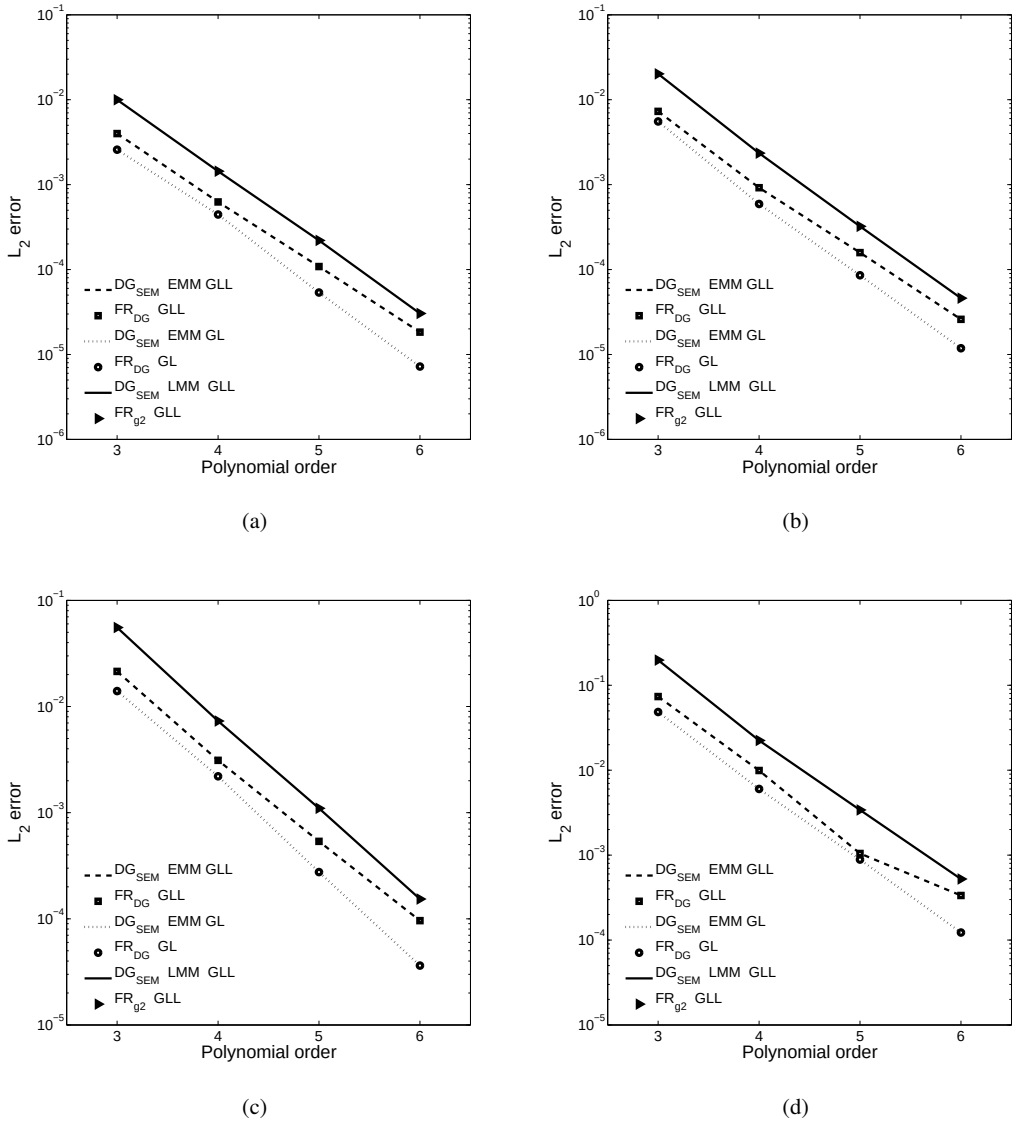

Figure 5. L^2 error vs polynomial order P on the deformed grid at the final time $T = 2s$. Figures (a)-(d) depict ρ, ρu, ρv and E respectively.

For a perfect gas the pressure is related to the total energy by the expression

$$E = \frac{p}{\gamma - 1} + \frac{1}{2}\rho(u^2 + v^2),$$

where γ denotes the constant ratio of specific heats of the gas and is equal to 1.4 for air. The solution was represented by a third, fourth, fifth and sixth order polynomials. First the polynomials were defined by a collocation projection of the solution values at four, five, six and ten GLL points for each element. Then the calculations were repeated using GL points. In all the cases a collocation quadrature rule was used for the inner product of the advection term of the DG scheme. With GLL both the cases of exact mass matrix (EMM) and lumped mass matrix (LMM) were considered. Periodic conditions were applied at the boundary of the grids. Periodic conditions were applied at

DOI: 10.1002/fld

the boundary of the grids, and an isentropic vortex in a free-stream flow (in the positive y direction) was prescribed within $\mathbf{\Omega}$ at $t = 0$:

$$\begin{aligned} \rho &= \left(1 - \frac{\beta^2(\gamma-1)e^{2f}}{16\gamma\pi^2}\right)^{\frac{1}{\gamma-1}}, \\ u &= \left(u_0 - \frac{\beta e^f (y-y_0)}{2\pi R}\right), \\ v &= \left(v_0 + \frac{\beta e^f (x-x_0)}{2\pi R}\right), \\ E &= \frac{\rho^\gamma}{\gamma-1} + \frac{1}{2}\rho\left(u^2+v^2\right), \end{aligned} \tag{30}$$

where

$$f = 1 - r^2,$$
$$r = \sqrt{(x-x_0)^2 + (y-y_0)^2}.$$

with $\beta = v_0 = 5$, $x_0 = y_0 = u_0 = 0$ and $r = 1$. An explicit Runge-Kutta time integration scheme of 4 stages is used to discretize the equations in time. The final time step was $T = 2s$, therefore the exact solution at the final time is equal to the initial of Eq. 30. The time step chosen was small enough in order to consider the temporal error negligible.

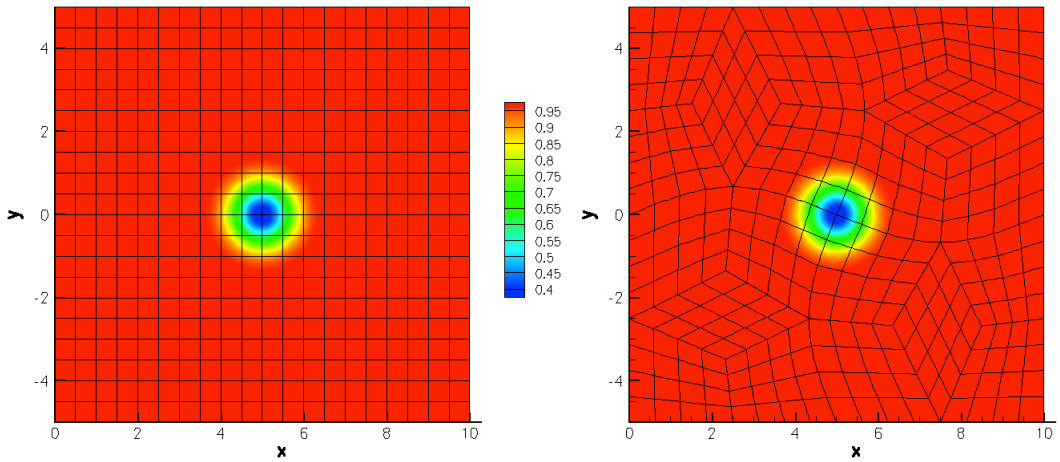

Figure 6. Solution at the final time $T = 2s$ for the simulation of the compressible Euler equations. The density contour is visualized on both the regular (left) and deformed (right) grids using seven GLL points.

As predicted by the mathematical derivation, figures 4 demonstrates that the appropriate DG and FR schemes exhibit identical numerical errors at the final time on a regular grid. As in the linear case Figure 5 also shows that the results match on the deformed grid because the approximation of the geometric factors is performed in the same way for both approaches. In particular we additionally note that the error produced with a collocation projection at GL points is minor when compared to GLL points. This is related to the property of GL points of minimizing the aliasing errors due to nonlinear flux functions, as shown in [13] and [11]. For both regular and deformed grids the results are identical up to machine precision. Figure 6 shows the solution at the final time on the regular grid and on the deformed grid.

DOI: 10.1002/fld

3.3. Comparison of computational time

In figure 7 a comparison between CPU processing time of different schemes is shown. In this figure we examine the average CPU time required for a timestep of a linear advection problem on the mesh of figure 1(a) using the FR_{g2} scheme, the DG_{SEM}-GLL with lumped mass matrix and the nodal $DG_{Q>P}$ scheme with exact mass matrix, where a quadrature rule with $Q > P$ was used for the inner product of the advection term. All of these scheme have solution values which are collocated at Gauss-Lobatto-Legendre points.

The solid and dashed lines represent two mathematically identical schemes and so we necessarily one might expect the same trend of CPU processing time. From the point of view of operations the schemes should all scale as P^3 and whilst a non-linear trend in polynomial order is obvious in the DG timings it is not clear for the FR scheme. We note the implementation based on the FR approach has a much better scaling with polynomial order suggesting it is better suited to the CPU architecture quite possibly due to a more efficient use of memory access thereby demonstrating the linear trend with polynomial order over the range considered in this plot. However, interestingly for low order expansions the implementation of the DG_{SEM}-GLL scheme performs better suggesting how the collocation nature of this scheme helps recover some of the inefficiencies that are likely to arise in the DG approach where integration over volume and trace spaces are necessary requiring addition computational cost and more complicated memory access. Since no attempt has been made

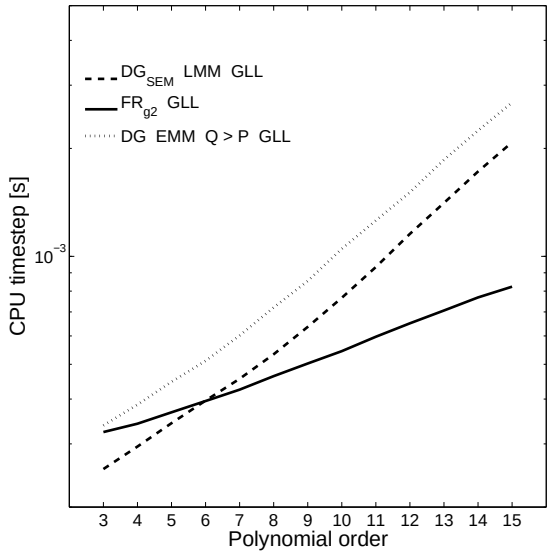

Figure 7. The CPU time required to calculate an average timestep of a scalar advection problem is shown as a function of polynomial order for three different schemes: DG_{SEM}-GLL, DG ($Q > P$) and FR_{g2}. The solution values are at Gauss-Lobatto-Legendre points in all cases.

to explicitly optimise the code, the differences between the DG_{SEM}-GLL and FR_{DG} are likely to be due to the different data structures used in the DG approach and in the FR. In particular, in the DG implementation contained in Nektar++, all the calculations are performed in the local element space (x, y), whilst using the second, all the calculations are in the standard element space (ξ, η). Further, in neither approach have we attempted to optimise the algorithm by calculating core operations over multiple element and this type of operations may also perform differently in each method. However, we note that in general that the efficiency of a solver is obviously highly dependent not only on the choice of scheme but also on its implementation, so that whilst some methods may be claimed as

DOI: 10.1002/fld

extremely efficient it is only through the consideration of detailed implementation issues that this claim could be corroborated.

4. CONCLUSIONS

The connections between three nodal versions of tensor product discontinuous Galerkin spectral element approximations and two types of flux reconstruction schemes were shown both through a mathematical derivation and a numerical study. It was demonstrated that, for a advection equation, the DG_{SEM} scheme with an exact mass matrix and the FR_{DG} scheme are equivalent on a quadrilateral grid. It was demonstrated that the DG_{SEM}-GLL scheme with a lumped mass matrix and the FR_{g2} scheme are equivalent for the case of a 1D conservation law. These equivalences are valid for both the case of linear and nonlinear flux. The $DG_{Q>P}$ scheme with an exact mass matrix recovers the FR_{DG} scheme only when the flux function is linear. In fact, when the flux is nonlinear, the aliasing issues due to the nonlinearities are minimised by the higher precision of the quadrature rule of the $DG_{Q>P}$ scheme and, so, there are differences with the FR_{DG} scheme. These results can be extended to higher dimensional grids. Additionally, the connections established here are always valid on regular grids regardless of whether the flux function is linear or nonlinear. However in the case of a deformed mesh, the equivalence of the scheme depends on the approximation of the geometric factors. Our future work will focus on further exploring the connections between FR and DG schemes on deformed grids both theoretically and numerically. We also want to further investigate the efficiency of different implementation strategies of these schemes.

ACKNOWLEDGEMENT

This work was supported by the Laminar Flow Control Centre funded by Airbus/EADS and EPSRC under grant EP/I037946. DM acknowledges support from the EU FP7 project IDIHOM under grant No. 265780. PV would like to acknowledge the Engineering and Physical Sciences Research Council for their support via an Early Career Fellowship (EP/K027379/1). SS additionally acknowledges Royal Academy of Engineering support under their research chair scheme.

REFERENCES

1. Reed, W.H., Hill, T.R. *Triangular mesh methods for the neutron transport equation*. Technical Report LA-UR-73-479, Los Alamos National Laboratory, Los Alamos, New Mexico, USA, 1973.
2. Cockburn, B., Shu, C. *RungeKutta discontinuous Galerkin methods for convection-dominated problems.* J. Sci. Comput. volume 16, 2001.
3. Arnold, D.N., Brezzi, F., Cockburn, B., Marini, L.D. *Unified analysis of discontinuous Galerkin methods for elliptic problems*. SIAM J. Numer. Anal., volume 39, 2001.
4. Huynh H.T. *A flux reconstruction approach to high-order schemes including discontinuous Galerkin methods.* 18th AIAA CFD Conference", 25-28 June 2007, Miami, FL.
5. Hesthaven, J.S., Warburton, T. *Nodal Discontinuous Galerkin Methods—Algorithms, Analysis, and Applications*. Springer, Berlin, 2008.
6. Kopriva, D.A., Kolias, J.H. *A conservative staggered-grid Chebyshev multidomain method for compressible flows*. J. Comput. Phys., volume 125, 1996.
7. Kopriva, D.A., Woodruff, S.L., Hussaini, M.Y. *Discontinuous spectral element approximation of Maxwells equations*. Discontinuous Galerkin Methods, Springer, 2000.
8. Liu, Y., Vinokur, M., Wang, Z.J. *Spectral difference method for unstructured grids I: basic formulation*. J. Comput. Phys., volume 216, 2006.
9. Vincent P.E. Castonguay P. Jameson A. *A new class of high-order energy stable flux reconstruction.* J Sci Comput 47:5072, 2011.
10. Castonguay P. Vincent P.E. Jameson A. *A new class of high-order energy stable flux reconstruction schemes for triangular elements.* J Sci Comput, 2011.
11. Castonguay P. Vincent P.E. Jameson A. *Application of high-order energy stable flux reconstruction schemes to the Euler equations.* AIAA Aerospace Sciences Meeting, Orlando FL, 4-7 January 2011.
12. Williams D.M. Castonguay P. Vincent P.E. Jameson A. *An extension of energy stable flux reconstruction to instead, nonlinear, viscous problem on mixed grids.* AIAA CFD Conference, Honolulu Hawaii, 27-30 June 2011.
13. Jameson A. Vincent P.E. Castonguay P. *On the nonlinear stability of the flux reconstruction schemes.* (2nd edn). J Sci Comput, 50:434445, 2012.
14. Allaneau Y. Jameson A. *Connections between the filtered discontinuous Galerkin method and the flux reconstruction approach to high order discretizations.* (2nd edn). Comput. Methods Appl. Mech. Engrg, 200:36283636, 2011.

DOI: 10.1002/fld

15. Gassner G. Kopriva D. A. *On the Quadrature and Weak Form Choices in Collocation Type Discontinuous Galerkin Spectral Element Methods.* J Sci Comput, 2010 volume 44(2).

DOI: 10.1002/fld